NASA Technical Memorandum 84362

NASA-TM-84362 19830018647

Aerodynamic Characteristics of Generalized Bent Biconic Bodies for Aero-Assisted Orbital-Transfer Vehicles

Carol B. Davies and Chul Park

May 1983

NASA
National Aeronautics and
Space Administration

NASA Technical Memorandum 84362

Aerodynamic Characteristics of Generalized Bent Biconic Bodies for Aero-Assisted Orbital-Transfer Vehicles

Carol B. Davies, Informatics General Corporation, Palo Alto, California
Chul Park, Ames Research Center, Moffett Field, California

National Aeronautics and
Space Administration

Ames Research Center
Moffett Field, California 94035

AERODYNAMIC CHARACTERISTICS OF GENERALIZED BENT BICONIC BODIES FOR AERO-ASSISTED, ORBITAL-TRANSFER VEHICLES

Carol B. Davies*
Informatics General Corporation, Palo Alto, California

and

Chul Park†
NASA Ames Research Center, Moffett Field, California

Abstract

A method was developed to generate the surface coordinates of body shapes suitable for aero-assisted, orbital-transfer vehicles (AOTVs) by extending bent biconic geometries. Lift, drag, and longitudinal moments were calculated for the bodies using Newtonian flow theory. These techniques were applied to symmetric and asymmetric aerobraking vehicles, and to an aeromaneuvering vehicle with high L/D. Results for aerobraking applications indicate that a 70°, fore half cone angle with a spherically blunted nose, rounded edges, and a slight asymmetry would be appropriate. Moreover, results show that an aeromaneuvering vehicle with L/D > 2.0, and with sufficient stability, is feasible.

Nomenclature

A = area projected by body (reference area)

C_d = drag coefficient

C_L = lift coefficient

D = total drag

i = index for body surface point

L = total lift

M = metacenter

N = total moment

$\hat{n}$ = body normal vector

P = surface point

p = pressure

R_{max} = maximum radius of body

R_n = blunt nose radius

s_D, s_L = moment arms at P

S_D, S_L = average moment arms

X_c = proportion of first cone length to total body length

(X_{cp}, Y_{cp}) = x and y coordinates of center of pressure

X_{sm} = initial smoothing location

$\underline{V}$ = free-stream velocity vector

V_∞ = free-stream velocity

α = angle of attack

α_{max} = maximum angle of attack for maintaining stability

γ = stability derivative = $dY_{cp}/d\alpha$

δ = angle between body normal and lift direction

θ_a = aft half cone angle

θ_b = angle between fore and aft cone axes (bend angle)

θ_f = fore half cone angle

$\theta_1, \theta_2, \theta_3$ = direction angles of body normal

ρ_∞ = free-stream density

ϕ = angle between body normal and flow direction

ω = edge smoothing width = $(X_c - X_{sm})/R_{max}$

Introduction

The effectiveness of the Space Shuttle can be enhanced if a new type of vehicle is developed with the ability to commute between various space satellites. The altitude of satellites, or space stations, varies from the current low Earth orbits to geosynchronous orbit. Such orbital transfer requires a vehicle that is capable of making altitude and synergetic (i.e., inclinational) orbital plane changes. The efficiency of this vehicle could be improved by making use of the Earth's atmosphere for some of its maneuvering. Such a vehicle is referred to as an aero-assisted, orbital-transfer vehicle (AOTV).[1] Several designs have been proposed for a vehicle capable of making orbital altitude changes. For altitude change alone, vehicles with low L/D, referred to as aerobraking vehicles, are currently being investigated.[1,2] However, for synergetic plane changes, a more appropriate vehicle would be one with a high L/D, which is referred to as an aeromaneuvering vehicle. Little work has been done on the investigation of the aerodynamic characteristics of these bodies. A bent biconic body has been proposed as a compromise to produce a moderately high drag, and a

---

*Consultant, Professional Services Operations West (PSOW).

†Research Scientist.

moderately high L/D.[3,4] Knowledge of the aerodynamic characteristics of a vehicle is necessary to make even a preliminary assessment of its mission performance. There is an urgent need to approximately assess a large range of possible geometries for their aerodynamic characteristics.

The purpose of the present work is to 1) develop a computer program that generates body coordinates and associated body-normal vectors for a class of body geometries; 2) generate configurations of body shapes that will have low L/D for orbital altitude changes and very high L/D for synergetic plane changes; and 3) produce quick estimates for lift and drag coefficients, moments, and stability margins for these varying shapes.

The work is focused on three types of geometries: 1) a symmetric, spherically blunted cone with a rounded frustum; 2) an asymmetric sphere cone, also with a rounded frustum; and 3) a low drag, high L/D lifting body. It is necessary to round the frustum for the geometries of 1) and 2) to overcome the very high heat transfer rates at the frustum's edge.[5] One serious problem with a symmetric shape is its lack of roll stability. An asymmetric body would have positive roll stability; this geometry is also examined in this work. It will be demonstrated that this asymmetric body can be designed with a sufficient stability for a wide range of angle of attack.

In the past, low drag and high L/D lifting bodies have generally been designed for terrestrial landing, and have not been configured for stowing in the Space Shuttle. The simplest high L/D shape is a flat plate; however, it is not aerodynamically stable. To produce aerodynamic stability, it is necessary to have a slight curvature on the lifting surface. Truncating a smoothed, generalized, bent biconic will produce such a body shape with high L/D and a curved lifting surface.

Calculation of Body Coordinates

The basic geometry of a generalized bent biconic is described by five variables. These are the fore half cone angle, θ_f; the aft half cone angle, θ_a; the angle between the two cone axes (bend angle), θ_b; the proportion of first cone length to total body length, X_c; and the nose radius, R_n, of the spherically blunted fore cone. Lengths are normalized with respect to the total body length measured from the apex of the first cone. Figure 1 shows a profile of a bent biconic with $\theta_f = 12.84°$, $\theta_a = 7°$, $\theta_b = 7°$, $X_c = 0.6$, and $R_n = 0.03$. The reference longitudinal axis is chosen to coincide with the fore cone axis. This is the x axis of the x-y-z coordinate system shown in Fig. 1. A body with these dimensions has been studied experimentally[4] and theoretically.[6] An additional feature of the code used in this study is the ability to smooth the sharp juncture between the two cones. This is controlled by an additional variable, X_{sm}, that defines the location on the x-axis where smoothing is to begin. The smoothed curve is defined as a fourth order polynomial with no first or third order term and with a continuous second derivative to ensure that the surface is uniquely defined by this single parameter.

These six variables can produce a wide range of body shapes, and some of these examples are seen in Fig. 2. The effect of smoothing the sharp juncture can be seen in Fig. 2a. Also shown is the option of truncating the end of the body perpendicular to either cone axis. Figure 2b shows the shape generated by truncating an upper portion of a biconic body. This truncation curve may be of a first or of a second order. The symmetric body seen in Fig. 2c is obtained when using a negative aft cone angle, a large nose radius, and the smoothing modification. The dotted line shows the effect of changing the smoothing parameter. In Fig. 2d a small bend angle has been introduced to produce an asymmetric body.

The solution of the equation of the common ellipse at the intersection plane is the first step in the procedure in obtaining the surface coordinates. The apex of the aft cone and other necessary parameters are then calculated and used for solving the analytical equations that describe the body surface. Figure 3 is an example showing cross sections at given x-stations for a body with $\theta_f = 10°$, $\theta_a = 20°$, $\theta_b = 15°$, and $R_n = 0.05$. These cross sections are circular along the fore cone, are part circular and part elliptical through the juncture area, and are elliptical until the end of the body. After obtaining the body coordinates, the body normal vector is calculated numerically at each body coordinate.

Aerodynamic Characteristics

One of the objectives of this work is to provide a quick and simple method for computing aerodynamic characteristics for a range of body shapes. This information can then be used to determine the flight performance of the vehicles. The aerodynamic characteristics are presented in terms of lift and drag forces. These were chosen to facilitate flight trajectory calculations and to circumvent the ambiguity of the body reference axis. The transformation from lift and drag forces to normal and actual forces is well known.

As with any atmospheric flight vehicle, an aeromaneuvering AOTV will perform in the same manner as a conventional airplane performs, and therefore the aerodynamic definitions of lift, drag, and moment apply. For an aerobraking vehicle, the performance criteria depend strongly on the mode of control. To correct for errors in entry angle, and for the uncertainty of atmospheric density, an aerobraking vehicle must be able to vary either lift or drag during its flight. The concept of drag modulation has been proposed and investigated.[7] To modulate drag, it is necessary to vary body geometry during flight, the feasibility of which has not yet been demonstrated. In the present work, the alternate concept of lift modulation is pursued. Since control surfaces are ineffective for a very blunt body, an alternative method for modulating lift must be found. The present work will investigate the feasibility of maintaining the required angle of attack by means of adjusting the center of gravity location. This adjustment could be performed by a hinge or gimbal motion. The vehicle must be stable at the achieved angle of attack; that is, a moment must be produced that will restore the angle of attack to the required value. It is therefore necessary to know

the stability characteristics of the aerobraking vehicle over a wide range of angles of attack. In this work, only longitudinal stability will be fully investigated; the inclusion of roll and directional stability is not addressed at this time.

Method of Calculation

Newtonian flow theory presents a reasonable approximation for pressure in the high Mach number flows encountered by an AOTV, and it is used in this work. In general, a surface is defined by its normal at every point. The angle between this normal and the direction of the oncoming flow can then be found. Defining this angle at a general surface point, i, as ϕ_i, the local pressure p_i is given by

$$p_i = \rho_\infty V_\infty^2 \cos^2(\phi_i)$$

where ρ_∞ is the free-stream density and V_∞ is the free-stream velocity. This expression is equivalent to the more familiar sine-squared formula.[8] Drag, which acts in the direction of the flow, is given by $p_i \cos(\phi_i)$, and lift, which acts in the direction normal to the flow, is given by $p_i \cos(\delta_i)$, where δ is the angle between the body normal vector and the lift direction. These angles are more clearly shown in Fig. 4a. The body normal vector in this same coordinate system

$$\hat{n} = \cos\theta_1 \underline{i} + \cos\theta_2 \underline{j} + \cos\theta_3 \underline{k}$$

where θ_1, θ_2, and θ_3 are direction angles with respect to x, y, and z axes and are shown in Fig. 4b. It should be noted that the directions of pressure, drag, and lift do not lie in the same plane. The integrated pressure, total drag, and total lift are obtained by summing their local values over the surface area that is impinged by the flow. Newtonian flow theory dictates that only the surface area directly wetted by the flow should be included in the surface integration. A point will be on this windward side if the angle between the flow and the body normal is less than 90°. The drag and lift coefficients are obtained by

$$C_d = 2D/\rho_\infty V_\infty^2 A$$

and

$$C_L = 2L/\rho_\infty V_\infty^2 A$$

where D and L are the total drag and lift, and A is the area projected by the body on the y-z plane.

Two cases were run to check the accuracy of the results obtained by using this method. The first was simply to check the code by calculating the drag coefficients of single cones with large nose radii. An excellent match was obtained when these were compared with the analytically derived drag coefficients for the same body dimensions. In the second test case, comparisons were made with the experimental results at Mach 6 for the bent biconic body shown in Fig. 1. Figure 5 shows drag and lift coefficients versus angle of attack for both methods. It can be seen that both agree to within approximately 5%. The L/D values agree extremely well. The small discrepancies can mainly be attributed to the non-Newtonian flow in the experiment. Newtonian flow theory presumes an infinite Mach number and a specific heat ratio of 1, and neglects wall friction. For quick estimates of the performance of a proposed body, however, these slight discrepancies are easily tolerated.

The diagram in Fig. 6 illustrates the technique used to compute the lift and drag moments of the body. Each surface point (shown as P in the diagram) is projected on the x-y plane. The moments for this projected line are taken about the system origin, where s_L is the moment arm for lift and s_D is the moment arm for drag. The total moments are found by summing each local moment over the appropriate body surface area, that is, total lift moment, $N_L = \Sigma\, s_{L_i} L_i$, and total drag moment, $N_D = \Sigma\, s_{D_i} D_i$. The signs of each s_{L_i} and s_{D_i} must be carefully monitored. The center of pressure (X_{cp}, Y_{cp}) is found by computing the average arm length by $S_L = N_L/L$ and $S_D = N_D/D$. These are then translated into the x-y plane. The computed horizontal center of pressure (X_{cp}) for each angle of attack is compared with the experimental results of Ref. 4, and plotted in Fig. 7. There is a fair agreement between the two sets of data. There is a discrepancy, however, that can be attributed partly to the unsuitability of the Newtonian flow for a body with a sharp juncture point. At such a juncture point, pressure transmission within the boundary layer reduces the pressure difference between the two surfaces. Although this phenomenon has a minimal effect on the total lift or drag, it does influence the moments. However, for the smooth surfaces considered in the remainder of this work, such discrepancies will be negligible.

The next step is to obtain permissable locations for the center of gravity. To do so, the center of pressure is plotted for each angle of attack. The resultant force line of the lift and drag forces that acts at the center of pressure is now drawn. Figure 8 shows examples of these lines. The point at which the resultant force meets the longitudinal axis is called the metacenter, M. To produce a particular angle of attack, the center of gravity should lie along the force line. The vehicle must be able to restore itself if a correction of angle of attack is required. A change in angle of attack will produce a change in the center of pressure, and consequently a change in the force line. This new force line will produce a moment in the restoring direction as long as the rate of change of Y_{cp} with respect to α (called the stability derivative, and defined as γ) remains sufficiently large and negative. The maximum angle of attack up to which γ maintains this condition will be referred to as α_{max}. The force line at α_{max} will therefore be the upper limit for the location of the center of gravity. The longitudinal location for the center of gravity is bounded by X_{cp} and M of this same force line. The quantities γ, α_{max}, and M therefore completely determine the stability characteristics of a vehicle and will be referred to frequently in the next section.

The code was written in FORTRAN for a DEC VAX/VMS system, and the average run time for a complete case was under 2 min.

Results

Aerobraking Vehicles

The aerodynamic characteristics computed for one case of a typical symmetric body are first described. Several parameters are then varied to provide information for generating an optimum body shape. All the data are normalized with respect to the maximum radius, R_{max}, of the body so that the results are presented in a comparable form for each body shape.

Symmetric Body Shape

A symmetric body with rounded frustum is seen in Fig. 8, with $\theta_f = 70°$, $\theta_a = -70°$, $R_n = 0.6$, and $X_{sm} = 0.24$. The lift and drag coefficients and L/D were computed for angles of attack between 0° and 40° and are shown in Figs. 9a and 9b. A fore cone angle >45° will produce negative lift values; the absolute values will be used in this report. C_d varied from 1.6 at $\alpha = 5°$ to 0.9 at $\alpha = 40°$, and $|C_L|$ varied between 0.1 and 0.5 for the same range. $|L/D|$ varied from a minimum of 0.07 at $\alpha = 5°$, to a maximum of 0.57 at $\alpha = 40°$. The variation of the center of pressure (X_{cp}, Y_{cp}) is seen in Figs. 9c and 9d. X_{cp} remained fairly constant at approximately 0.41 up to $\alpha = 30°$, and then increased rapidly to 0.46 at $\alpha = 40°$. Y_{cp} decreased linearly up to $\alpha = 30°$ and then flattened out. In Fig. 9e, M remained between 1.6 and 1.65 up to $\alpha = 25°$ and then decreased rapidly. The stability derivative also remained fairly constant up to 25° with a value of approximately 0.29; however, the decrease that is seen for $25 < \alpha < 30$ indicates that this is the maximum α for maintaining stability. From these results, the maximum angle of attack (α_{max}) for this body shape is close to 25°. At α_{max}, $|L/D| = 0.35$.

To assess the effect of change on the nose radius, cases were run for R_n/R_{max} varying from 0.3 to 2.4, with all other parameters unchanged. The results were quite similar to the case already described. Figure 10a illustrates that although the stability derivative was a maximum for $R_n/R_{max} = 1.0$, the overall change was not significant until $R_n/R_{max} > 2.0$. Plotted on the same graph is the variation M with respect to R_n/R_{max}. Initially, M also remained fairly constant, then increased for the larger nose radii. Both curves are only valid up to α_{max}. $|L/D|$ at α_{max} varied very little, maintaining a value between 0.35 and 0.37. These results indicate that the nose radius has little effect on the characteristics of the body, although γ does decrease for large values of R_n/R_{max}.

Another body parameter of interest is the roundness of the frustum edge. The change in radius of curvature is controlled by X_{sm}/R_{max}, the location where smoothing is to begin. The smoothing width, $\omega = (X_c - X_{sm})/R_{max}$, is the distance between the cut line and X_{sm}, and as this decreases, the frustum edge becomes sharper, that is, the smallest X_{sm} produces the most rounded edge. This effect can be seen in Fig. 2c where the solid line was produced by a greater smoothing width than the dotted line. Cases were run varying ω from 0.08 to 0.38. The results of this variation can be seen in Fig. 10b. As ω increased, γ also increased, indicating that the more rounded frustum edge produced a significantly more stable body. At the same time, M decreased. This implies that the more stable bodies have a smaller range for locating the center of gravity. The maximum angle of attack remained at 25°, whereas $|L/D|$ varied from 0.31 for the most rounded edge to 0.39 for the sharpest.

Increasing or decreasing the fore half-cone angle, θ_f, had a significant effect on the range of the stability derivative, and on the location of M. Cases were run for $\theta_f = 60°$ and 80° for comparison with the 70° results above. It was difficult to match the body dimensions for true comparisons; nevertheless, a clear picture emerged. Figure 11 shows some interesting results. With increasing θ_f, M increased from 1.5 at 60° to 2.25 at 80° (Fig. 11a), whereas γ decreased from 0.35 to 0.19 (Fig. 11b). Even more interesting, α_{max} increased to 35° for $\theta_f = 60°$ and decreased to a very low 15° for the 80° case. As a consequence, $|L/D|$ at α_{max} is greatest for the 60° case (Fig. 11c). The range of $|L/D|$ was more dependent on the body shape than on the other variables; Fig. 11c also indicates the range of $|L/D|$ for each cone angle.

These data show that the fore cone angle has a significant effect on the stability of the vehicle. An angle of 70° appears to be the optimum fore cone angle for this type of aerobraking vehicle. A fore cone angle of 60° restricts the location of the center of gravity to a fairly small range; however, it has a greater stability derivative. For the 80° case, $\alpha_{max} = 15°$ would almost certainly be too low.

Asymmetric Body Shape

The characteristics of axially asymmetric bodies were also examined in this work. Figure 12 is a profile of such an asymmetric body with $\theta_f = 70°$, $\theta_a = -70°$, $\theta_b = 5°$, $R_n = 0.96$, and $X_{sm} = 0.26$. Because of asymmetry, the characteristics were evaluated for angles of attack between -40° and +40°. The values computed for C_d, $|C_L|$, and $|L/D|$ were very close to the values for the similarly proportioned symmetric case. The M for each force line no longer lies on the longitudinal axis as this is not the symmetric axis of the body. In this figure, M lies above the longitudinal axis at a point where most of the force lines meet. This is at a value approximately equal to 1.6. Figure 13 is a plot of γ versus angle of attack. Between $-25 < \alpha < 25$, the stability derivative remained fairly constant at a value ≈ 0.28, again indicating an $\alpha_{max} \approx 25°$.

To find the effect of changing the bend angle, the same case was run for $\theta_b = 3°$, 7°, and 10°. When the stability derivatives were compared with the 5° case, very little change had occurred; γ remained between 0.27 and 0.28. The M slightly increased with increasing bend angle. This indicates that the bend angle can probably be chosen to best suit the other requirements of the vehicle, particularly for maintaining its roll stability. The amount of bend angle required for this roll stability needs further investigation.

The effect of a fore cone angle change was also investigated, and, as in the symmetric case, exact comparisons could not be made. However, the same general picture was produced: The larger

cone angle of 60° generated a larger stability derivative and a smaller M. The range for α_{max} again ran from 35° for $\theta_f = 60°$ to 15° for $\theta_f = 80°$.

In conclusion, the introduction of a small bend angle to a symmetric aerobraking vehicle will have little effect on the longitudinal stability.

Aeromaneuvering Vehicle

The concept of creating a high lift, high L/D vehicle by truncating a bent biconic body was introduced earlier in this report. This truncated body is the lower segment of the intersection of a second order equation with a bent biconic body. The equation is defined by three given points on this upper surface. An example is shown in Fig. 14, where the shaded portion is the truncated body. The finalized body shape must fulfill several requirements. These are:

1) The body should be proportioned for utilizing the cargo bay of the Space Shuttle (approximately 20 by 5 m) as efficiently as possible.

2) The rear side area must be large enough to produce yaw and roll stability.

3) The under surface must be sufficiently curved to produce longitudinal stability.

With these constraints in mind, the chosen body shape, seen in Fig. 15, was determined by trial and error. The biconic surface was generated from a body with $\theta_f = 10°$, $\theta_a = 10°$, $\theta_b = 5°$, $X_{sm} = 0.4$, and $X_c = 0.6$. The three points defining the upper surface equation were (0.3 - 0.05), (0.6 - 0.095), and (1.0 - 0.13). The three views of the body seen in Fig. 15 are plotted to the same scale. The lower curved surface can be seen with the greatest volume in the rear (Fig. 15a). It is clear that the sharp leading edges will require some form of active cooling. The upper dotted portion, which indicates the dead air region at $\alpha = 0$, can be filled without affecting the aerodynamic characteristics. This dead air region would increase when the vehicle flies at a finite angle of attack. Also shown are the force lines for $5° < \alpha < 30°$. Figure 15b is the view from above, showing a large area on the upper surface, and Fig. 15c is the view from the front, showing the area projected on the y-z plane. Figure 16 details the aerodynamic characteristics computed for this aeromaneuvering vehicle. In Fig. 16a, the range of L/D is from 7.2 at zero angle of attack to 1.4 at $\alpha = 30°$. A sufficient spread in X_{cp} is required to provide the required stability margin. The computed values of X_{cp} presented in Fig. 16b indicates a sufficient spreading up to an α_{max} approximately equal to 20°. At this α_{max}, L/D still maintains a value of 2.0.

The volume to carry fuel and cargo must be found within the dead-air region on the lee side of the vehicle. The actual cargo-carrying volume will be determined by the intended maximum L/D: the higher this L/D, the smaller the angle of attack, leading to a smaller cargo volume. Eventually, the cargo-carrying volume will be so small that the vehicle will be unable to carry all of its own fuel internally. Additional fuel could be provided by external fuel tanks. Figure 17 indicates how the vehicle and two fuel tanks could efficiently utilize the Space Shuttle cargo bay. Finally, a sequence of events is proposed for the vehicle to perform its journey from the Space Shuttle to another orbiting body. These steps, shown in Fig. 18, are:

1) The vehicle is deployed from the Shuttle cargo bay, with the external fuel tanks attached.

2) The rocket engines ignite and the vehicle begins its journey toward the Earth's atmosphere.

3) The empty fuel tanks are jettisoned and the vehicle enters the atmosphere.

4) Using its designed maneuvering capabilities, the vehicle banks and turns into its new orbit.

5) The vehicle exits the atmosphere and rendezvous with a satellite.

Because of the large L/D of this vehicle, the required amount of fuel for performing aeromaneuvering will be quite small. It may even be possible to make two plane changes in one mission, thereby enabling the vehicle to reach its destination and return to the Space Shuttle.

Conclusions

Symmetric and asymmetric aerobraking bodies and an aeromaneuvering body can be generated by generalized bent biconic geometry. The aerodynamic characteristics derived for these bodies using Newtonian flow theory were shown to be sufficiently accurate for preliminary design studies.

For aerobraking bodies, a 70° half cone angle provided the best compromise between longitudinal stability and center of gravity location. The introduction of a small asymmetry to a symmetric body had little effect on the aerodynamic characteristics. For an aeromaneuvering vehicle, it is possible to design a body that has an $L/D > 2$ and which can still maintain a positive stability margin.

References

[1]Walberg, G. D., "A Review of Aeroassisted Orbit Transfer," AIAA Paper 82-1378, Aug. 1982.

[2]Schmitt, D. A., "Base heating on an Aerobraking Orbital Transfer Vehicle," AIAA Paper 83-0408, Jan. 1983.

[3]Florence, D. E., "Aerothermodynamic Design Feasibility of a Generic Planetary Aerocapture/Aeromaneuver Vehicle," AIAA Paper 81-1127, June 1981.

[4]Miller, C. G., Blackstock, T. A., Helms, V. T., and Midden, R. E., "An Experimental Investigation of Control Surface Effectiveness and Real-Gas Simulation for Biconics," AIAA Paper 83-0213, Jan. 1983.

[5]Kemp, N. H., Rose, P. H., and Detra, R. W., "Laminar Heat Transfer Around Blunt Bodies in Dissociated Air," Journal of Aeronautics and Space Sciences, Vol. 26, No. 7, July 1959, pp.

[6]Swaminathin, S., Kim, M. D., and Lewis, C. H., "Three-Dimensional Nonequilibrium Viscous Shock-Layer Flows over Complex Geometrics," AIAA Paper 83-0212, Jan. 1983.

[7]Andrews, D. G., Caluori, V. A., and Bloetscher, F., "Optimization of Aerobraked Orbital Transfer Vehicles," AIAA Paper 81-1126, June 1981.

[8]Hayes, D. W. and Probstein, R. F., "Hypersonic Flow Theory," Applied Mathematics and Mechanics, Vol. 5, Academic Press, 1959, p. 73.

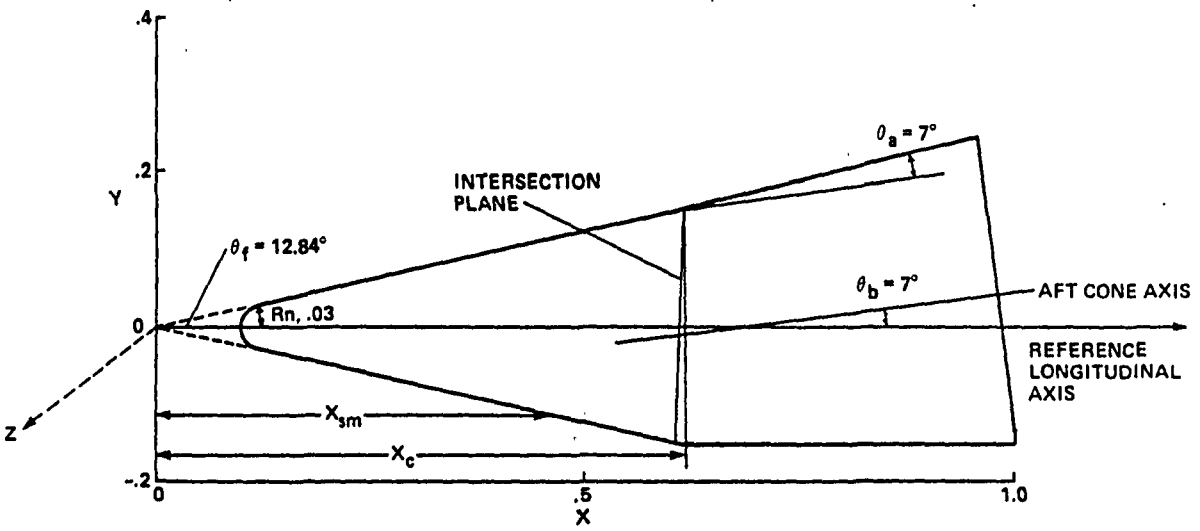

Fig. 1 Bent Biconic with $\theta_f = 12.84°$, $\theta_a = 7°$, $\theta_b = 7°$, $R_n = 0.03$, and $X_c = 0.6$.

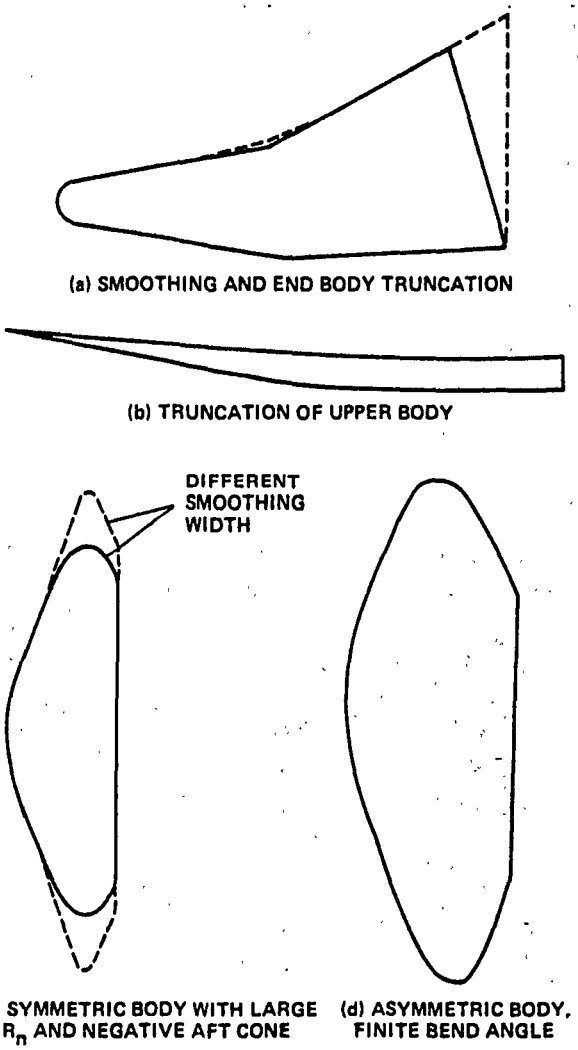

Fig. 2 Generalized, bent biconic body shapes. (a) Optional smoothing and end body truncation; (b) Truncation of upper body; (c) Symmetric body with large R_n and negative aft cone angle; (d) Asymmetric body, finite bend angle.

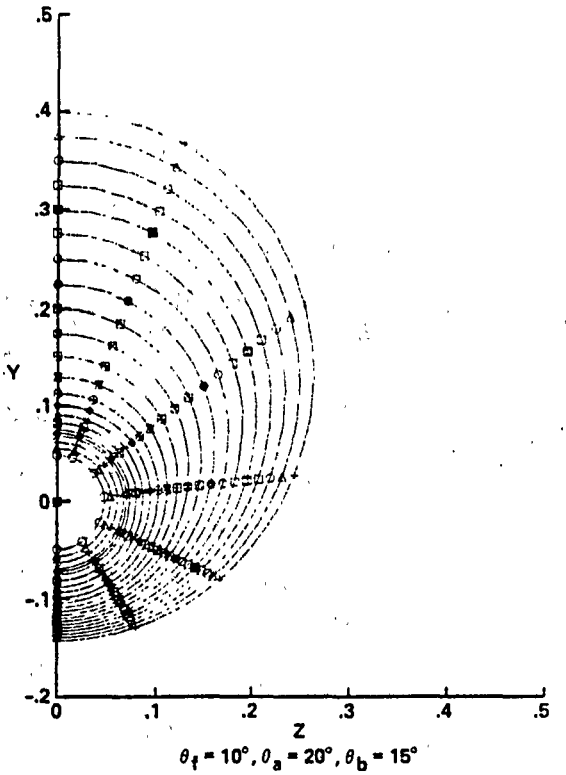

Fig. 3 Cross section of bent biconic with $\theta_f = 10°$, $\theta_a = 20°$, $\theta_b = 15°$.

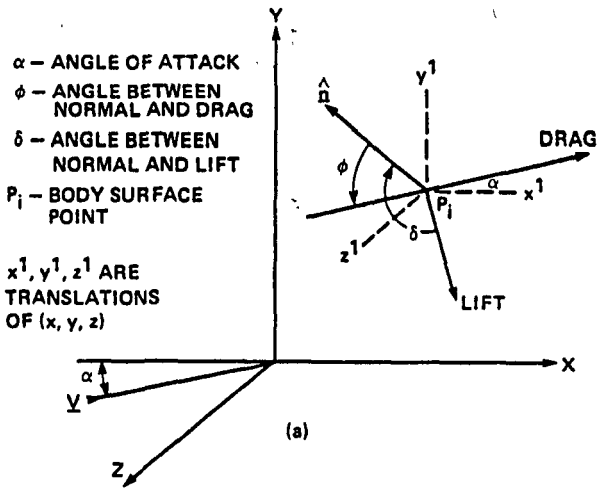

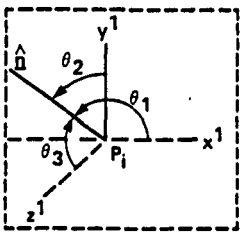

DIRECTION COSINES OF BODY NORMAL AT SURFACE POINT P_i

$\hat{n} = \cos\theta_1 i + \cos\theta_2 j + \cos\theta_3 k$

(b)

Fig. 4 Lift and drag forces at body surface point P.

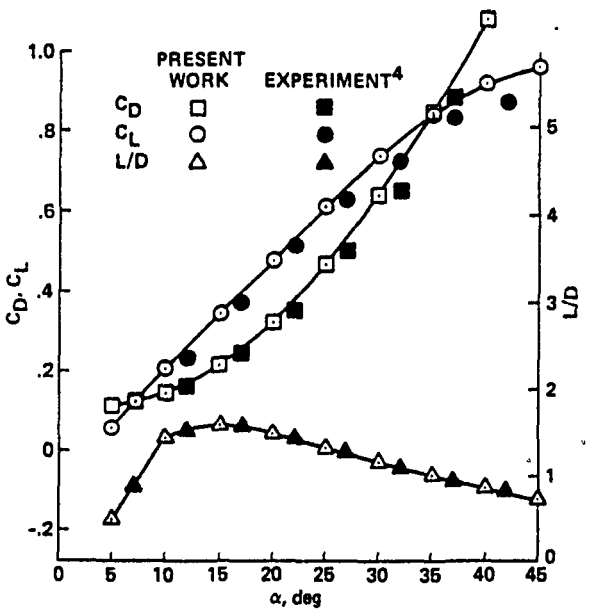

Fig. 5 Comparison of lift and drag coefficients and L/D with experimental results for body seen in Fig. 1.

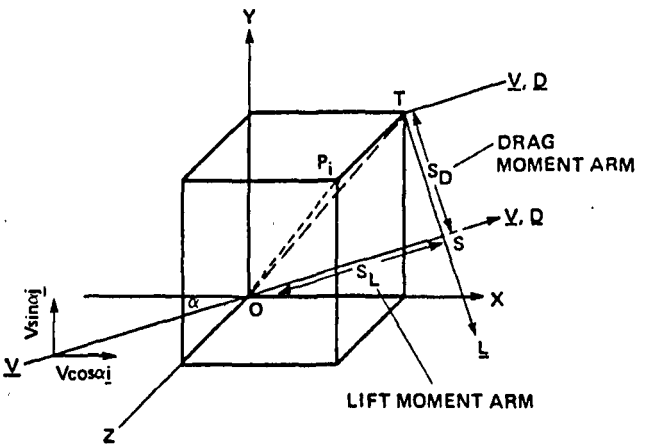

Fig. 6 Computation of moments; OT is the projection of OP onto the x-y plane.

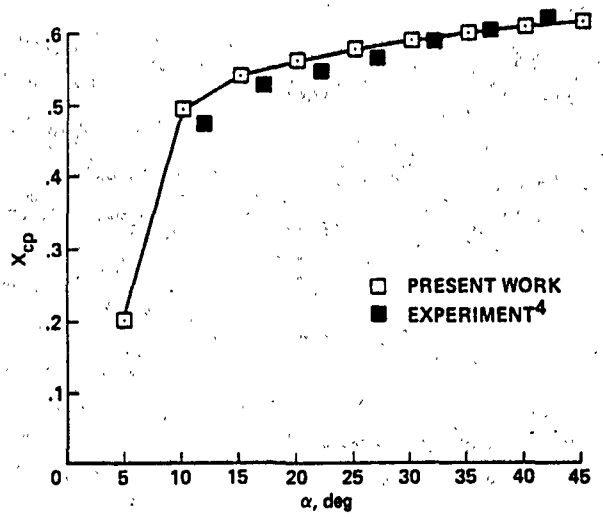

Fig. 7 Comparison of calculated center of pressure with experimental data for body seen in Fig. 1.

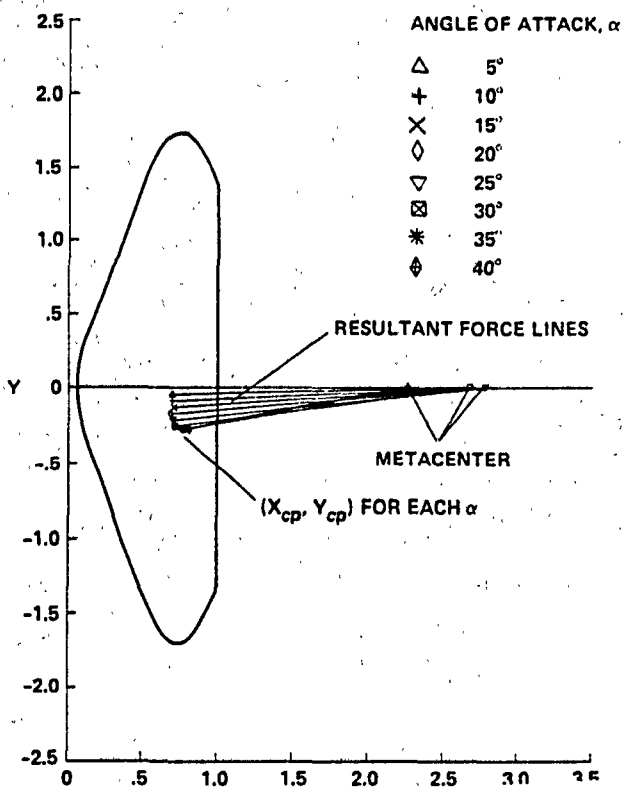

Fig. 8 Symmetric aerobraking body with $\theta_f = 70°$, $R_n/R_{max} = 0.6$, $X_{sm}/R_{max} = 0.24$.

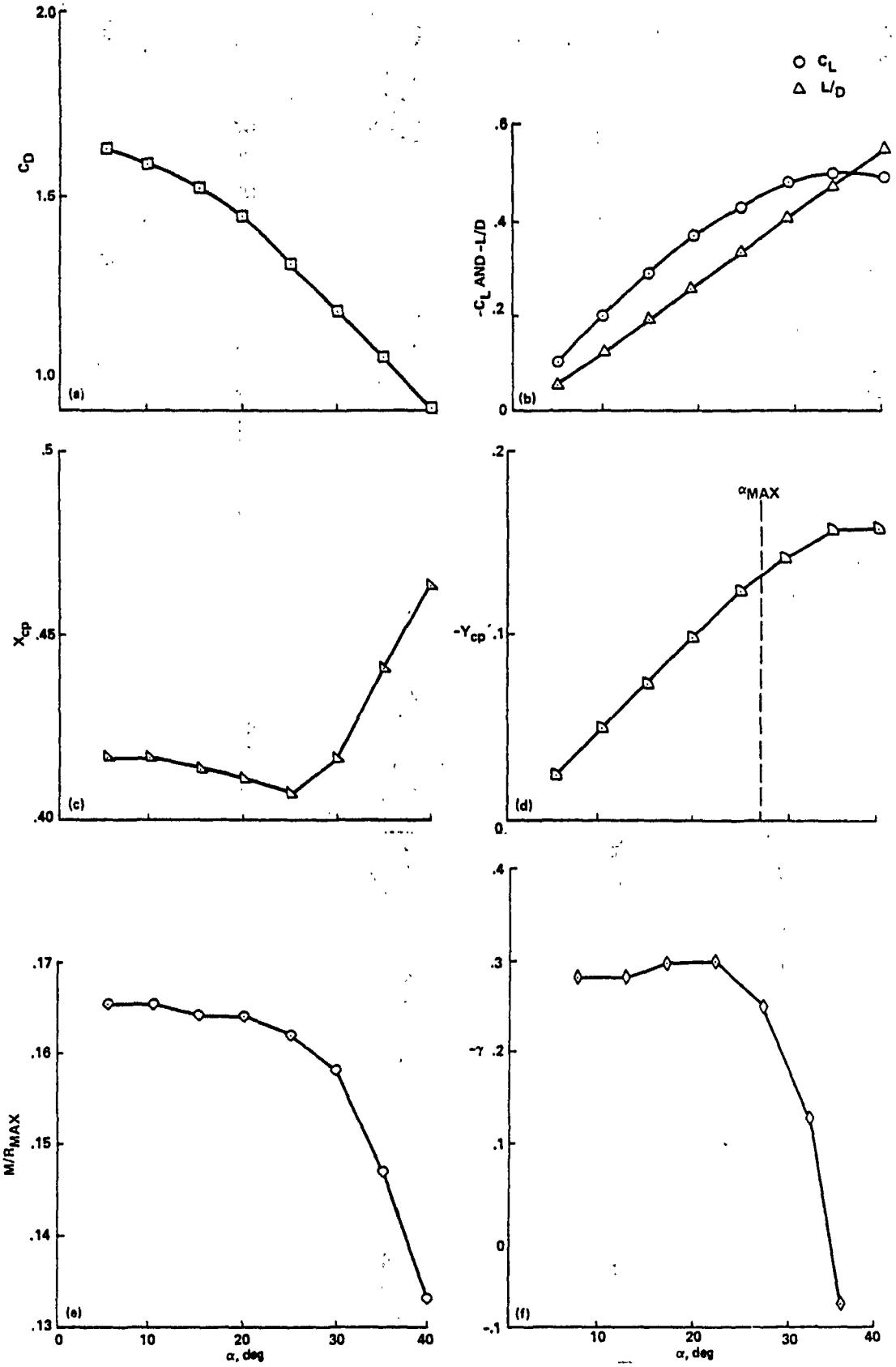

Fig. 9 Aerodynamic characteristics of body in Fig. 8.

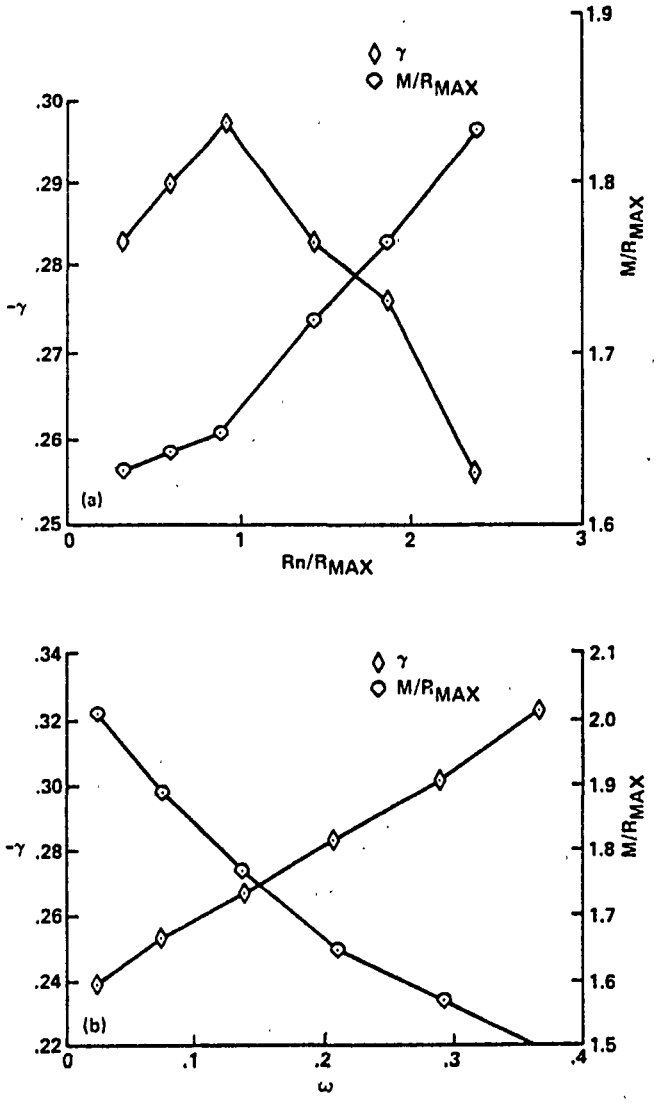

Fig. 10 Variation of nose radius and smoothing width for body in Fig. 8.

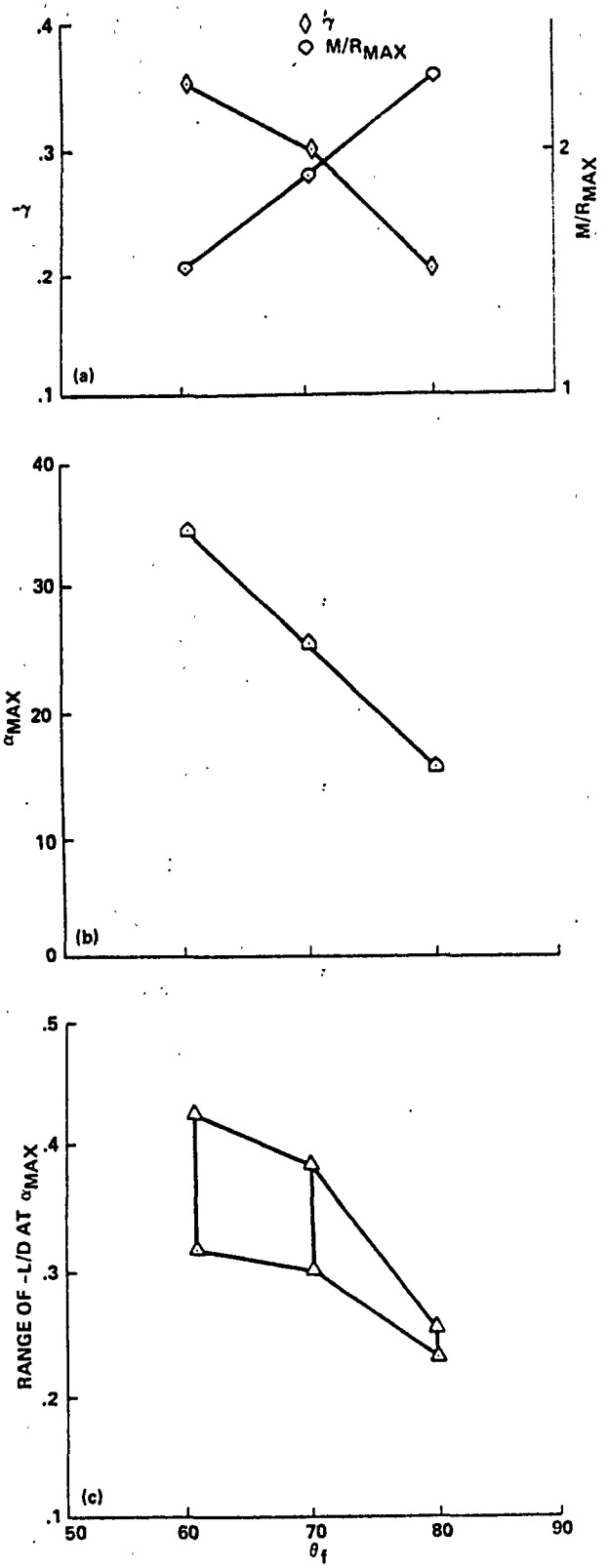

Fig. 11 Effect of change in half cone angle for symmetric bodies.

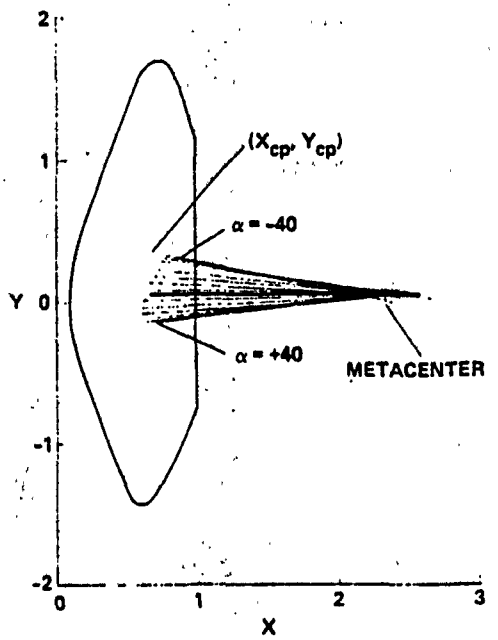

Fig. 12 Asymmetric body with $\theta_f = 70°$, $\theta_b = 5°$, $R_n = 0.96$, $X_{sm} = 0.26$ (showing the lines of force).

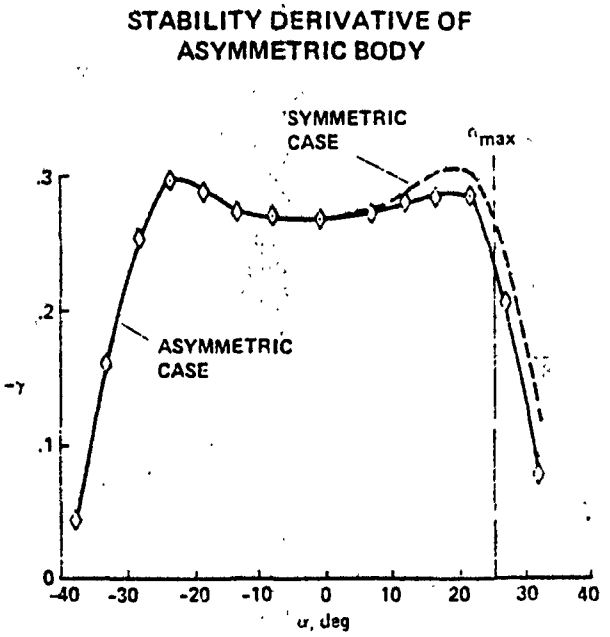

Fig. 13 Stability derivative for body in Fig. 12.

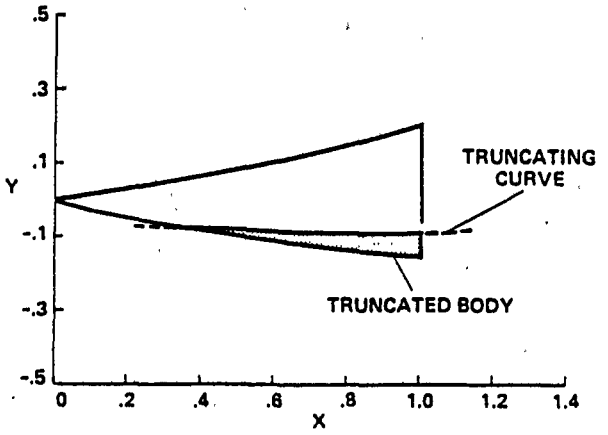

Fig. 14 Truncated portion of a bent biconic with $\theta_f = 10°$, $\theta_a = 10°$, $\theta_b = 5°$, $X_c = 0.7$, $X_{sm} = 0.4$.

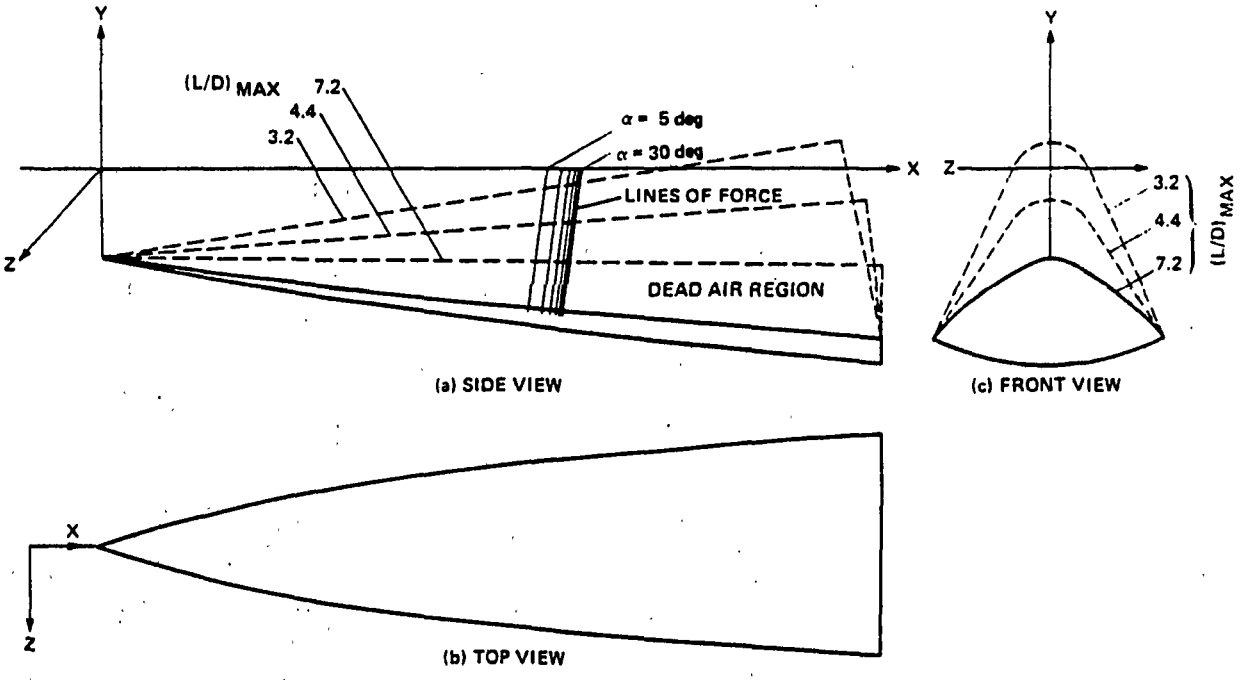

Fig. 15 Three views of an aeromaneuvering vehicle.

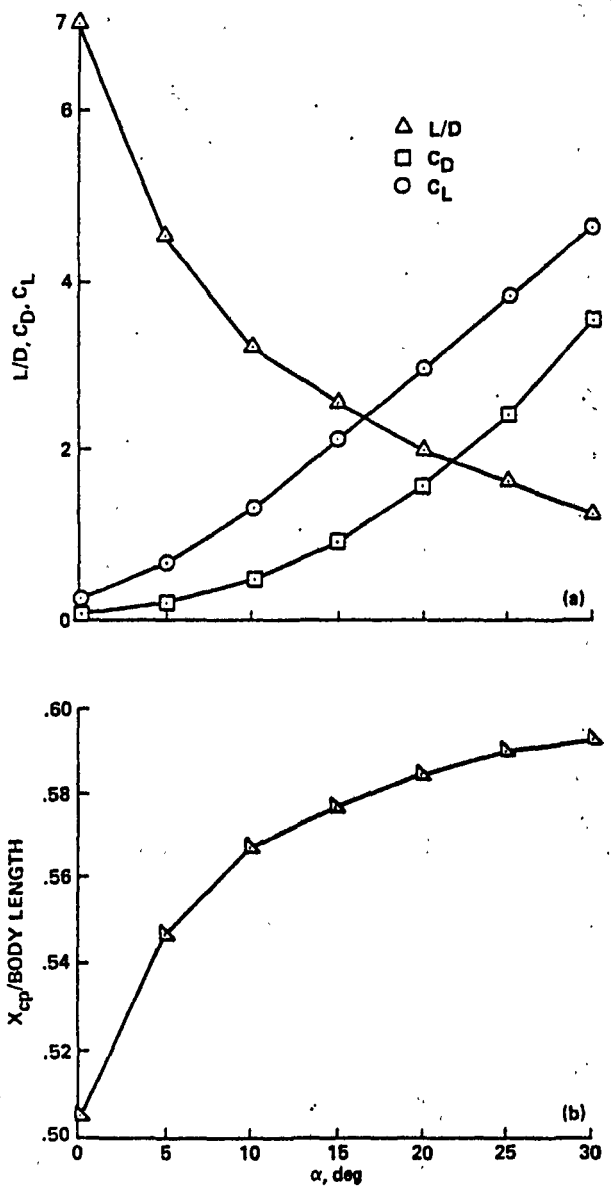

Fig. 16 Aerodynamic characteristics for truncated body shown in Fig. 15.

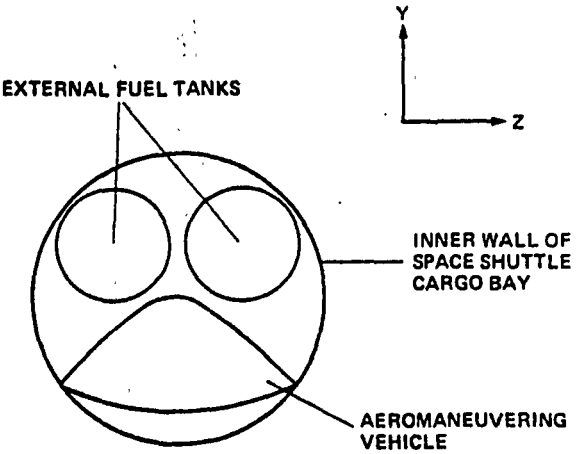

Fig. 17 Accommodation of the aeromaneuvering vehicle (Fig. 15) within the Space Shuttle cargo bay.

AEROMANEUVERING MISSION

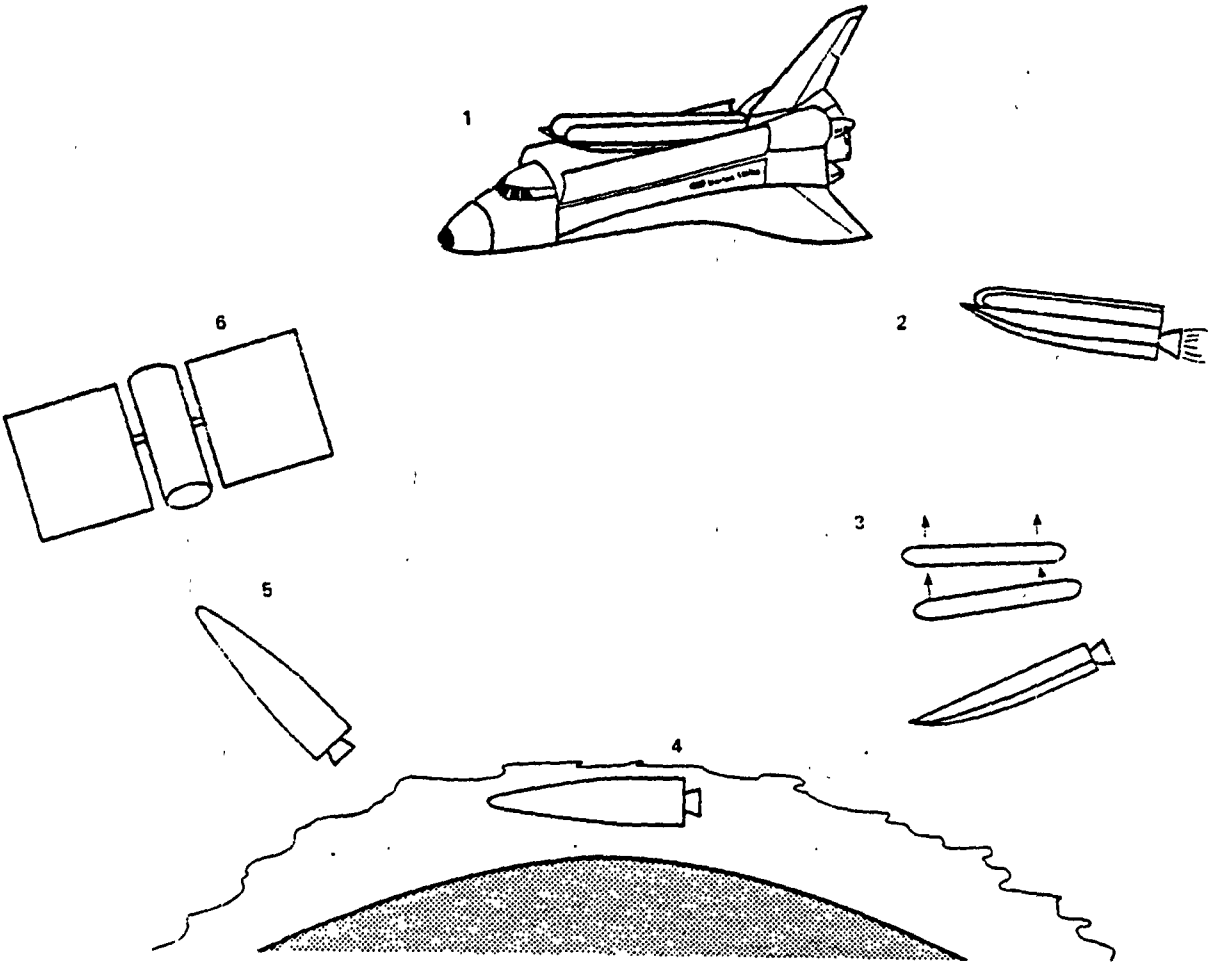

1. Report No.	2. Government Accession No.	3. Recipient's Catalog No.
NASA TM-84362		

4. Title and Subtitle	5. Report Date
AERODYNAMIC CHARACTERISTICS OF GENERALIZED BENT BICONIC BODIES FOR AERO-ASSISTED, ORBITAL-TRANSFER VEHICLES	April 1983
	6. Performing Organization Code

7. Author(s)	8. Performing Organization Report No.
Carol B. Davies* and Chul Park**	A-9281
	10. Work Unit No. T-6465

9. Performing Organization Name and Address	11. Contract or Grant No.
*Informatics General Corporation, Palo Alto, Calif. **Ames Research Center, Moffett Field, Calif.	
	13. Type of Report and Period Covered
12. Sponsoring Agency Name and Address	Technical Memorandum
National Aeronautics and Space Administration Washington, D.C. 20546	14. Sponsoring Agency Code

15. Supplementary Notes

Point of Contact: Carol B. Davies, Ames Research Center, M/S 229-4, Moffett Field, Calif. 94035, (415) 965-6204, FTS 448-6204

16. Abstract

A method was developed to generate the surface coordinates of body shapes suitable for aero-assisted, orbital-transfer vehicles (AOTVs) by extending bent biconic geometries. Lift, drag, and longitudinal moments were calculated for the bodies using Newtonian flow theory. These techniques were applied to symmetric and asymmetric aerobraking vehicles, and to an aeromaneuvering vehicle with high L/D. Results for aerobraking applications indicate that a 70°, fore half cone angle with a spherically blunted nose, rounded edges, and a slight asymmetry would be appropriate. Moreover, results show that an aeromaneuvering vehicle with L/D > 2.0, and with sufficient stability, is feasible.

17. Key Words (Suggested by Author(s))	18. Distribution Statement
Hypersonic aerodynamics Stability and control Space transport system Spacecraft design	Unlimited Subject Category - 18

19. Security Classif. (of this report)	20. Security Classif. (of this page)	21. No. of Pages	22. Price*
Unclassified	Unclassified	18	A02

*For sale by the National Technical Information Service, Springfield, Virginia 22161